ORNL/TM-2017/504

Status Report Documenting Development of Friction Stir Welding for Joining Thin Wall Tubing of ODS Alloys

David T. Hoelzer
Maxim N. Gussev
Jeffrey R. Bunn

September 29, 2017

OAK RIDGE NATIONAL LABORATORY
MANAGED BY UT-BATTELLE FOR THE US DEPARTMENT OF ENERGY

ORNL/TM-2017/504

Nuclear Technology Research and Development (NTRD) Program

Status Report Documenting Development of Friction Stir Welding for Joining Thin Wall Tubing of ODS Alloys

D.T. Hoelzer, M.N. Gussev and J.R. Bunn

Oak Ridge National Laboratory

Date Published: September 29, 2017

Prepared by
OAK RIDGE NATIONAL LABORATORY
Oak Ridge, Tennessee 37831-6283
Managed by
UT-BATTELLE, LLC
for the
US DEPARTMENT OF ENERGY
under contract DE-AC05-00OR22725

CONTENTS

Page

LIST OF FIGURES

LIST OF TABLES

ACKNOWLEDGMENTS

This research was sponsored by the U.S. Department of Energy, Office of Nuclear Energy, for the Nuclear Technology Research and Development (NTRD) program.

The authors are grateful to Tom Geer for assistance in preparation of the SS-Mini tensile specimens fabricated from the stir zone and base metal regions of the friction stir welded thin plate of 14YWT. The authors want to also acknowledge Dr. Kevin Field for reviewing the manuscript.

ABSTRACT

The development of friction stir welding (FSW) for joining thin sections of the advanced oxide dispersion strengthened (ODS) 14YWT ferritic alloy was initiated in Fuel Cycle Research and Development (FCRD), now the Nuclear Technology Research and Development (NTRD), in 2015. The first FSW experiment was conducted in late FY15 and successfully produced a bead-on-plate stir zone (SZ) on a 1 mm thick plate of 14YWT (SM13 heat). The goal of this research task is to ultimately demonstrate that FSW is a feasible method for joining thin wall (0.5 mm thick) tubing of 14YWT.

To assess the quality of the FSW parameters used in the initial experiment, the tensile properties and plastic deformation behavior of miniature specimens that were fabricated from the SZ and base metal (BM) regions of the 14YWT plate were investigated by in-situ tensile testing and characterized using digital image correlation (DIC) techniques. The results of the DIC analysis showed that the strength properties of the specimens from the SZ decreased ~13% compared to specimens from the BM, but that the ductility properties were essentially unchanged by FSW. All specimens exhibited similar deformation behavior that consisted of increased intensity of strain localization and local strain rates in the region of the specimen gauge where necking occurred until the specimen failed. The results suggested that deformation bands may be slightly more prevalent during deformation in specimens from the SZ compared to the BM. Overall, the FSW parameters used to produce the bead-on-plate weld in the 1 mm thick plate of 14YWT were nearly optimized.

The microstructural analysis of the SZ presented in the FY16 milestone report indicated that several cracks oriented horizontally to the plane of the thin plate were observed in the SZ, thermal mechanically affected zone (TMAZ) and base metal (BM) on the retreating side of the weld. These cracks may have formed by the combination of stress introduced by friction stir welding (FSW) from clamping and residual stresses from FSW in the weld. For this reason, a HFIR Neutron Scattering User proposal was submitted and accepted for investigating residual stresses in the four plates of 14YWT that were produced during fabrication of the 1 mm thick plate. The results showed that residual strains accumulated in each plate with increasing rolling deformation magnitude. The dependence of the residual strains on orientation within the plates was obtained by scanning each plate in the extrusion (ED), rolling (RD) and normal (ND) directions. The results indicated that residuals strains increased in ED and RD with increasing deformation magnitude but were insensitive to the deformation magnitude in ND. This observation was consistent with deformation occurring in plane in the plates during rolling. The estimate of residual stresses in the final 1 mm thick plate of 14YWT used in the FSW study showed a range in values from ~122 - 384 MPa, which is a substantial amount of stress that could account for the pop-in crack that occurred during fabrication of tensile specimens for the DIC study. Additional residual stress measurements are planned in the next FY work package that will investigate the SZ to determine what how much residual stresses are produced by FSW and will study what effects post weld heat treatments have on reducing the residual stresses.

.

1. INTRODUCTION

Friction stir welding (FSW) is a solid-state joining technique originally developed within the aluminum industry in 1991. The FSW process involves plunging a rotating tool consisting of a pin and shoulder into the seam between two work pieces followed by translating along the seam to be joined. Heat is produced by friction from contact between the rotating tool and work pieces that softens the material and allowing it to flow around the tool during the translation of the rotating tool. As the tool travels along the seam, a cavity forms at the rear that is filled by forging material that is redistributed by the rotating tool and forms the weld. The redistribution process causes the material to experience extreme levels of plastic deformation and thermal exposure that, in turn, can have a significant effect on microstructural changes in the weld zone. FSW is considered a solid-state joining technique since the temperatures resulting from frictional heating that lead to welding of work pieces by plastic deformation lie below the melting temperature of materials.

The advanced ODS 14YWT ferritic alloy is being investigated in the NTRD program for thin wall fuel cladding in fast nuclear reactor technologies. The goals of this program are to develop fabrication methods for thin wall tubing and welding methods for joining thin wall tubing of 14YWT. For this research task, FSW is being developed for joining thin wall tubing of 14YWT which represents a major challenge due to issues with preserving the salient microstructure features of 14YWT that provide the high-temperature performance properties and radiation tolerance. The development of FSW for joining thin sections of 14YWT was initiated in 2015. The first FSW experiment successfully produced a bead-on-plate stir zone (SZ) on a 1 mm thick plate of 14YWT. Preliminary characterization studies of the SZ showed that the FSW parameters used to produce the bead-on-plate weld were nearly optimized. The results of the microstructural characterization studies showed that the grain structure in the SZ was increased slightly in size and was isotropic in shape compared to the highly elongated grains observed in the base metal (BM) of the 1 mm thick 14YWT plate and that nano-size Y-Ti-O oxide particles in the SZ exhibited slight coarsening in size. In the previous fiscal year (FY16), the tensile properties of specimens fabricated from the BM was initiated. This report covers the tensile properties and deformation behavior of specimens fabricated from both the SZ and BM that were obtained by digital image correlation during in-situ tensile testing of the specimens and residual stress data obtained from rolled plates of 14YWT with different deformation magnitudes that were produced during fabrication of the 1 mm thick 14YWT plate used in the FSW experiment.

2. MATERIALS AND EXPERIMENTAL

2.1. Friction stir welding

The initial FSW run produced a bead-on-plate stir zone (SZ) on a 0.1 cm thick plate of 14YWT as shown in Figure 1. The advancing and retreating sides of the spinning pin tool are shown in the Figure, in this case the pin tool traveled in the direction of the advancing side. From optical inspection, the weld zone showed good microstructure mixing with no evidence of coarse defects such as cavities. The swirl flow pattern observed for the SZ is commonly observed with FSW joints, which indicates that sufficient heat from friction generated between the rotating and traveling shoulder and pin tool with the 14YWT plate caused material to be redistributed from the front to the rear (retreating side) of the SZ.

2.2. In-situ tensile tests

Miniature tensile specimens referred to as SS-Mini were fabricated from the SZ and BM regions to investigate the tensile properties and local deformation behavior of the material [1]. The SS-Mini specimen used in this study is shown in Figure 2. The specimens had an overall length of 7 mm and thickness of 0.4-0.6 mm with a gauge that is 3.55 mm long and 0.8 mm wide (Fig. 2 left). The specimens were machined with the gauge aligned inside the SZ parallel to the FSW tool traveling direction. Three specimens were prepared from the SZ and two from the adjacent BM plate of 14YWT. The top surface of each specimen

was polished to 1200 grit finish. The tensile tests were performed on an MTS tensile screw machine at room temperature using displacement control and a corresponding strain rate of ~1 x 10^{-3} s^{-1}.

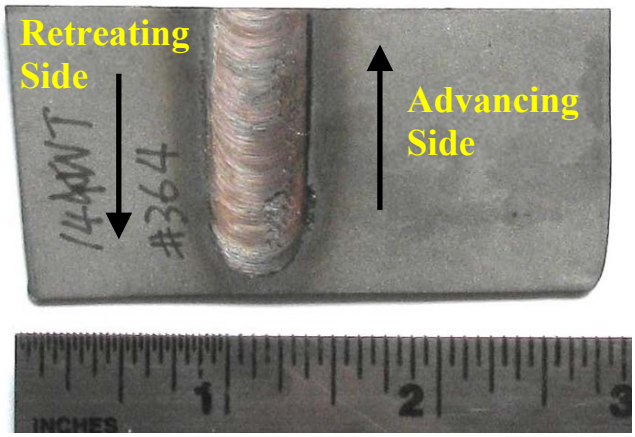

Figure 1. Optical image showing the bead-on-plate weld zone obtained by FSW on the 0.1 cm thick plate of 14YWT.

Digital image correlation (DIC) was used during the tensile tests. In this approach, the surface of the SS-Mini specimen is painted with speckles using black and white paints to measure localized extensions, or strain, along the gauge during the tensile test (Fig. 2 right). Digital images are recorded as a function of time during the tensile test. Figure 2 shows the specimens with the surface coating prior to testing. The tests were conducted by shoulder loading the specimens; images were taken using high-resolution Allied Vision GX3300 camera. The camera lenses provided a resolution ~5 μm per pixel over the gauge of the specimens. Strain fields and true stress-true strain curves were calculated using a VIC-2D commercial software and a custom program utilizing common DIC algorithms. The red line superimposed on the gauge of the specimen (Fig. 2) represents the region that the DIC analysis was conducted during tensile test.

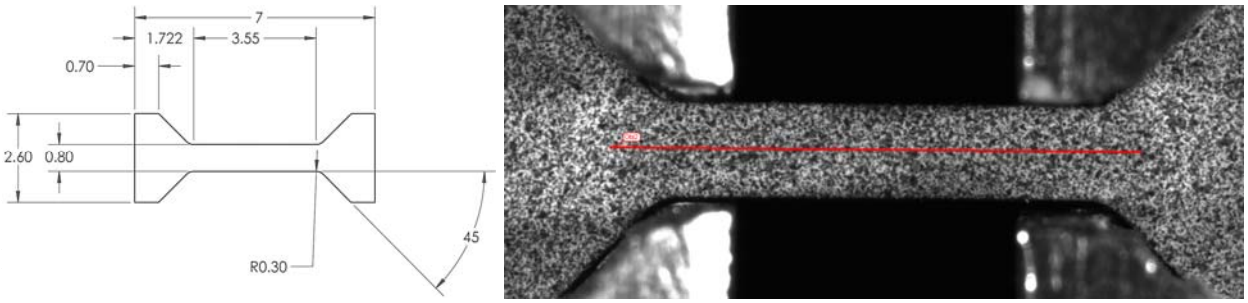

Figure 2. Drawings (left, dimensions are in millimeters [1]) and typical digital image of the SS-Mini tensile specimen (right) showing the surface coating and the superimposed line on the gauge section that is used in the DIC analysis.

2.3. Residual stress measurements

Neutron diffraction experiments were performed on the 4 plates of 14YWT that were fabricated for producing the 1 mm thick plate used in the FSW bead-on-plate weld. Each plate contained a different thickness and magnitude of deformation due to hot rolling at 1000ºC. The thickness and deformation magnitude of each plate determined from the reduction in thickness from the extruded bar (2.1 cm thick) were 10 mm and ~48% ($^{\#}$1), 5 mm and 76% ($^{\#}$2), 2.2 mm and 89% ($^{\#}$3) and 1 mm and 95% ($^{\#}$4), respectively.

The rolling directions for producing the plate samples for #1, #2 and #4 were normal to the extrusion direction while that of #3 was parallel to the extrusion direction.

The residual stress measurements were conducted on the HB-2B beam line at the Neutron Residual Stress Facility at HFIR. This research was associated with the ORNL Neutron Science User proposal (IPTS-18043.1) titled "The Role of Deformation Magnitude During Hot Rolling of 14YWT Plates on Generation of Residual Stresses" that was awarded beam time in December 2016. The objective of the study was to collect strain data in the form of 2-D plane of points to measure the magnitude and spatial distribution of strain as a function of deformation in the plate samples and to determine if the rolling direction played any role in the build-up of residual stresses. The sample goniometer allowed for spatial scanning of strains at different depths of each plate due to the different sample thicknesses ranging from 0.1 to 1.0 cm. Since the entire plate of each sample contained a similar magnitude of deformation induced by rolling, obtaining the strain-free lattice parameter "d-zero" value could not be obtained from a location on the plate where the residual stress may be viewed as small. Therefore, a separate sample of 14YWT (SM13 heat) was prepared for use as the d-zero location when recording the neutron diffraction runs. The results obtained from analyzing the residual stress data of the rolled plates will provide valuable data for comparing with similar measurements that will be conducted on samples prepared from the FSW SZ of a butt joint of the thin 14YWT plate in future experimental runs.

3. RESULTS AND DISCUSSION

3.1 Tensile property and deformation studies

The location and orientation of five SS-Mini tensile specimens relative to the stir zone on the 1 mm thick 14YWT plate are shown in Figure 3. Numbers for the specimens are superimposed on the plate shown in the figure. The SS-Mini specimens labeled #1 and #2 were located on opposite sides of the centerline in the SZ while specimen #3 was closer to the edge of the boundary between the SZ and thermal mechanically affected zone (TMAZ). The location of specimen #3 indicated that it most likely contained material of the SZ on the top and of the TMAZ on the bottom of the specimen, which may affect the tensile properties, but should not affect the deformation behavior during the tensile test since the DIC technique only analyzes the surface of the specimen, i.e. speckled coating. Specimens #4 and #5 were located in the BM region of the thin 14YWT plate.

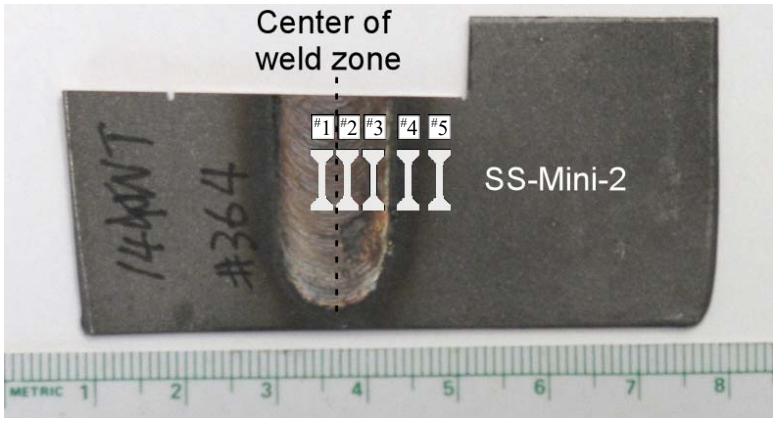

Figure 3. Template showing the layout of tensile specimens that were attempted to be fabricated from the 1 mm thick plate of 14YWT containing the bead-on-plate SZ.

Engineering stress-strain curves obtained from the tensile tests conducted on the SS-Mini specimens at room temperature are shown in Figure 4. The values obtained for the yield stress (YS), ultimate tensile

stress (UTS), uniform elongation (UE) and total elongation (TE) are compiled in Table 1. The specimens from the SZ (#1 and #3) showed YS and UTS values that were ~13% lower than those of specimens from the BM (#4 and #5). However, the ductility differences between the SZ and BM specimens were negligible. No tensile results were obtained for specimen #2 since it failed in the elastic zone during the tensile test. The reason for this failure is not understood since this specimen was fabricated on the opposite side of the centerline in the SZ that specimen #1 was fabricated. Since specimen #1 showed good ductility, it is possible that a flaw in the microstructure of the SZ such as the horizontal cracks FY16 milestone reported (M3FT-16OR020302031) was responsible for failure of specimen #2.

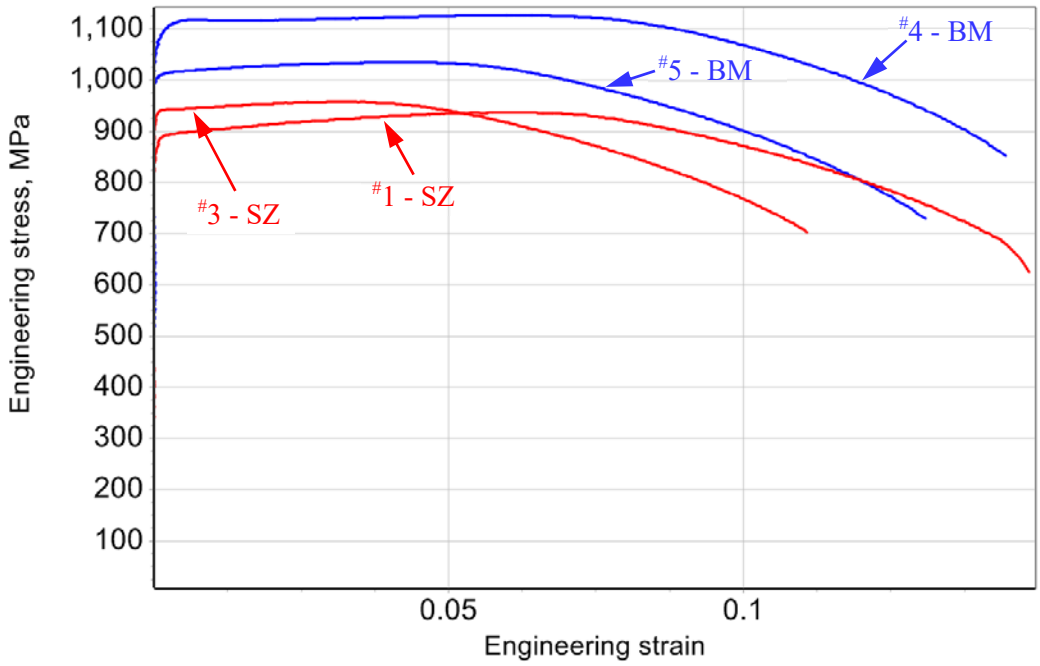

Figure 4. Engineering stress-strain curves of four SS-Mini specimens of 14YWT.

Table 1. Tensile properties of the SS-Mini specimens of 14YWT.

Specimen No.	Location	Yield stress, MPa	Ultimate stress, MPa	Uniform elongation, %	Total elongation, %
1	Stir Zone	892.1	937.2	5.87	14.83
2	Stir Zone	Failed before yielding			
3	Stir Zone	942.5	958.1	3.09	11.07
4	Base Metal	1095.7	1126.55	6.07	14.44
5	Base Metal	1012.7	1034.76	4.24	13.07

The deformation behavior of the SS-Mini specimens obtained by DIC analysis during the tensile test is illustrated for specimen #1 in Figure 5. This specimen was fabricated from the SZ. The insert observed in Figure 5a shows the pre-tested SS-Mini specimen with the surface coating of droplets and the superimposed line (red) along the gauge length representing the location of the strain distribution that was measured by DIC. The plot of von Mises strain as a function of position along the specimen gauge length is shown in Figure 5a. The experimental tensile curve shown in Figure 5b shows the 5 points were the distribution of strain was measured along the specimen gauge during the tensile test. The results indicated that strain was nearly homogeneous immediately after yielding, but became progressively more localized in the left region

of the gauge with further plastic deformation. The strain localization intensified in this region after reaching the uniform strain, which resulted in plastic instability, or necking, until failure of the specimen.

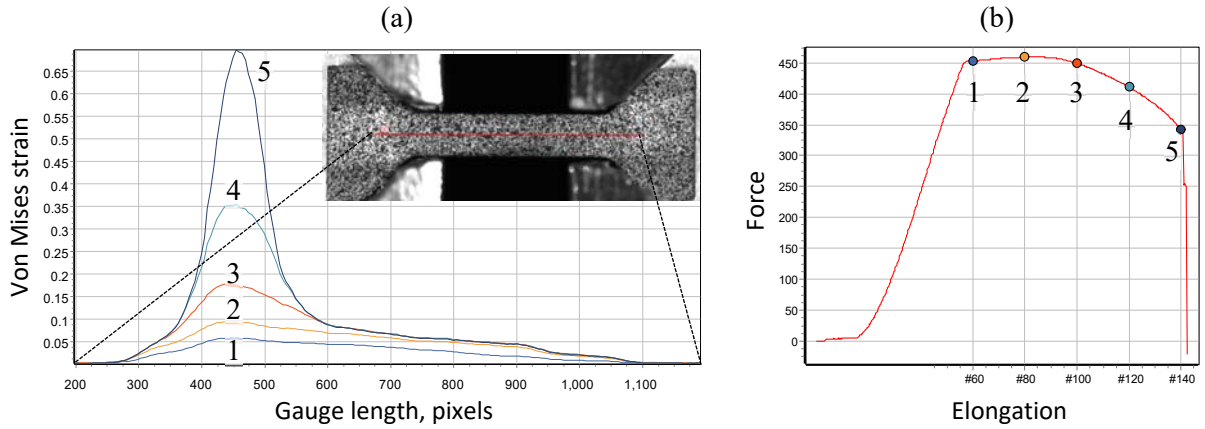

Figure 5. Specimen #1 from SZ. (a) Strain distribution (von Mises strain, Green-Lagrange strain tensor) along the specimen gauge at different time (Frame #). (b) Experimental tensile curve with force and elongation values for every image. *Insert shows superimposed line of DIC analysis on specimen gauge.*

The DIC results obtained for specimens #3, #4 and #5 are shown in Figure 6. Like specimen #1 (Fig. 5), specimens #3, #4 and #5 exhibited strain localization on the gauge during the tensile tests and that the strain localization always occurred away from the center of the gauge towards the shoulder. All the specimens showed only a small amount of homogeneous deformation after yielding. However, the distribution of strain after yielding appeared to cover larger lengths on the gauge for specimens #4 and #5 from the BM region compared to specimens #1 and #2 from the SZ region. However, once plastic instability occurred, the strain localization intensified on the gauge until the specimen failed.

Strain rate maps of the specimen gauges were obtained by DIC during the tensile tests. In this case, the displacement between each pixel during a time interval (Δt) based the image acquisition rate and crosshead speed gives the average displacement rate of each pixel composing the strain rate map. The strain rate maps of specimens #1, #3, #4 and #5 are shown in Figure 7. The horizontal axis of the images shows the distribution of strain rates obtained by DIC line analysis over the gauge length and the vertical axis represents the time from the start of the tensile test to specimen failure. The intensity scale is the computed strain rates of the data with red for low strain rates and white for high strain rates. The approximate points in time when the specimen reached the YS and UTS are marked in the images. The results indicated that a sudden increase in strain rates occurred in localized positions on the gauge of each specimen shortly after yielding that corresponded to the position where necking occurred later in the tensile test. The localized high strain rates for specimen #1 and to a lesser extent specimen #3 appeared to propagate along the specimen gauge during the tensile test before dissipating. After the specimens reached the UTS, the strain rates increased in a localized region of the gauge where necking was initiated. The localized strain rates increased rapidly as necking proceeded until the specimen failed.

The high spatial displacement resolution of DIC provided insight into the evolution of strain and strain rate during tensile deformation of the specimens fabricated from the 1 mm thick 14YWT plate. Strain localization occurred on the gauge section of each specimen that was always located away from the center of the gauge towards the grip section of the specimens. It is difficult to assess whether inhomogeneity in the microstructure between the SZ and BM played a role in the location and intensification of strain in each of the specimens. Pertaining to the strain rate maps (Fig. 7), the early spike in strain rate that was observed early in the tensile tests may be due to changes in the grain structure and dispersion of nanocluster by the

sudden nucleation and mobility of dislocations as deformation bands after yielding. These deformation bands then propagate along the gauge and appear to vary between each of the four specimens. The two SZ specimens showed a more pronounced propagation of the deformation band along the gauge compared to the BM specimens. These differences may be due to variations in the grain texture in the SZ caused by FSW compared to the BM. Regardless of the actual mechanism, the DIC data correctly accounted for the location and intensification of strain during the tensile tests on the advanced ODS 14YWT alloy.

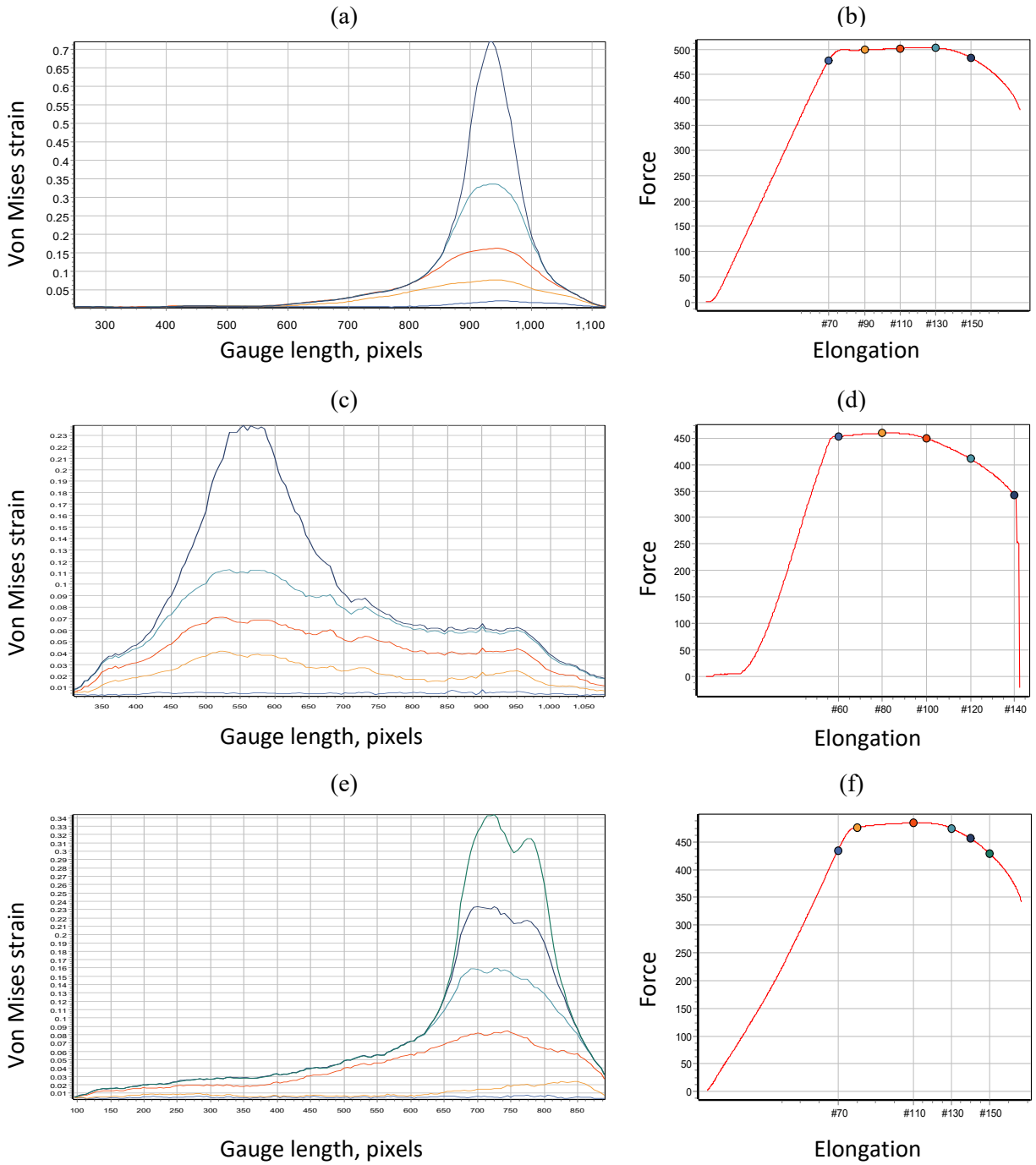

Figure 6 (a, b) Specimen #3, (c, d) Specimen #4 and (d, e) Specimen #5. (a, c, d) Strain distribution (von Mises strain, Green-Lagrange strain tensor) along the specimen gauge at different time (Frame #) and (b, d, f) experimental tensile curves with force and elongation values for all images.

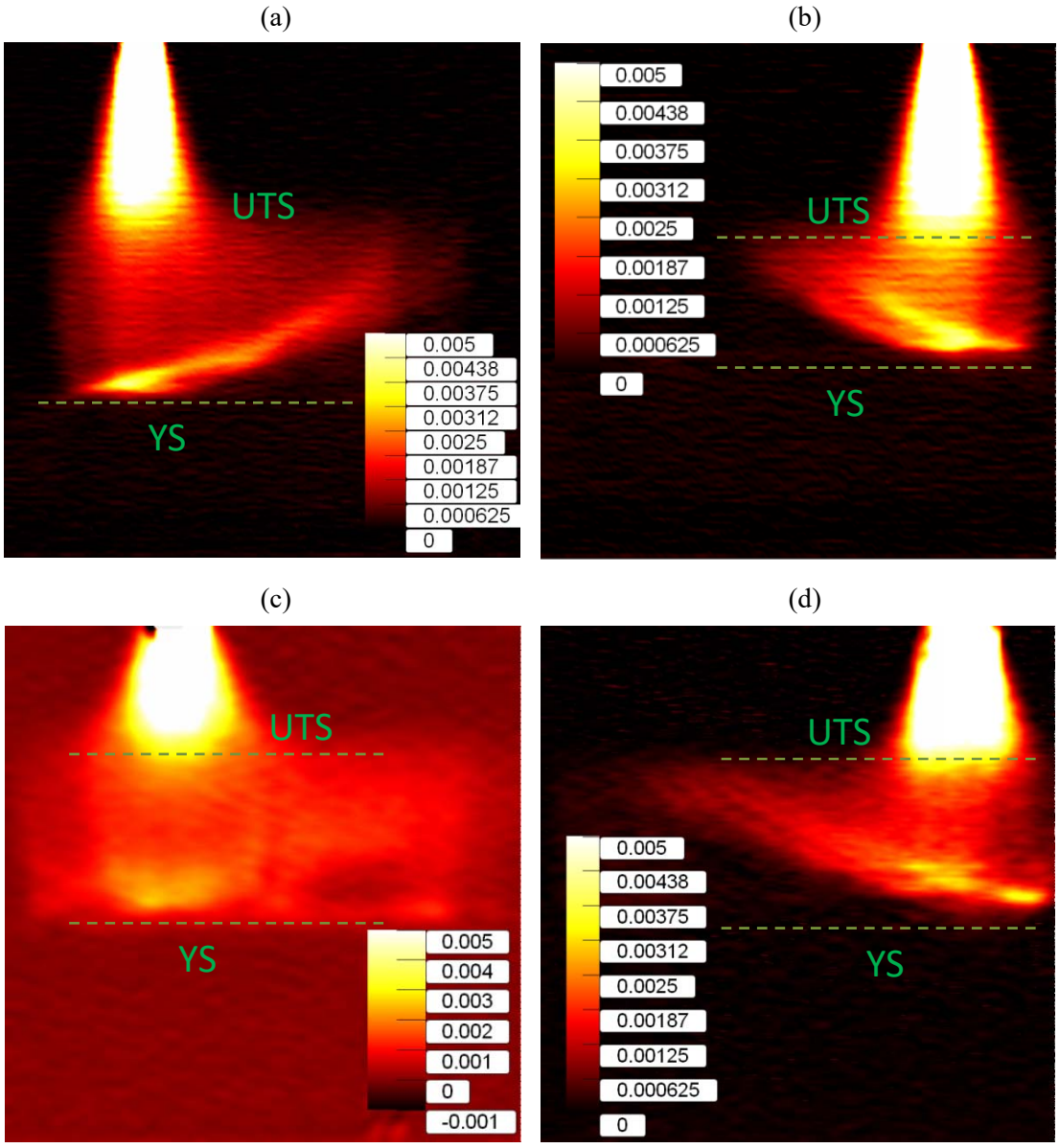

Figure 7. Strain rate maps of specimens (a) #1, (b) #3, (c) #4 and (d) #5.

3.2 Residual stress study

The reasons for investigating the residual stresses that may be present in the SZ of the 1 mm thick plate of 14YWT are due to two observations that were obtained from the microstructure characterization study and the fabrication of the SS-Mini specimens.

Figure 8 shows a composite of three optical microscopy (OM) images obtained from a region of the FSW bead-on-plate SZ that contained cracks on the retreating side. A large crack was observed to emanate from the bottom surface of the thin plate and several approximately horizontal cracks located in the SZ, TMAZ and BM regions of the microstructure. The horizontal cracks were not consistent with being pores since they were oriented horizontally in the microstructure normal to the rolling plane of the plate. This type of crack orientation was not found in a review of published FSW studies of a variety of alloys. The mechanism responsible for formation of the horizontal cracks most likely was related to residual stresses that could

have been caused by FSW as well as deformation induced by rolling the plate from 10 mm to 1 mm thickness in 4 steps.

Several FSW studies have investigated residual stresses in the stir zone of alloys [2-5]. In the studies of PM2000 [2] and MA956 [3], the longitudinal residual stresses near the surface showed M-shape profiles with tensile stresses across the stir zone centerline and tensile maxima occurring in the TMAZ regions that change to compressive stresses towards the HAZ and base metal regions. Brewer et al. [3] showed that different FSW conditions related to relative heat input led to variations in the magnitude of the longitudinal and transverse residual stresses in the weld zone. Their study also showed that the longitudinal tensile stresses that were measured as a function of depth remained nearly constant near the stir zone centerline but decreased in magnitude from the surface to a depth of 1 mm (4 mm thick plate) at a distance of 2 mm from the stir zone centerline. A similar observation was obtained by Ji et al. [5] in the friction stir weld of 7075 Al-alloy. In this study, the residual stresses were compressive near the mid-layer of the plate thickness and changed to tensile towards the top and bottom surfaces of the 12.3 mm thick plate. Based on these studies, it seems likely that residual stresses developed in the 1 mm thick 14YWT plate and that tensile stresses near the surface could have assisted in the formation of cracks that then propagated horizontally.

The texture induced from hot rolling the 14YWT plate by 95% RIT to 1 mm thickness could have also played a role in the horizontal crack propagation via a delamination mechanism. This type of fracture mechanism was recently published by Alam et al. [6] who showed that rolling produced a {100}<110> texture in the FCRD-NFA-1 (a new, larger heat of 14YWT) plate, which favors brittle cleavage in BCC alloys. It is not known how the cracks were nucleated, but along with the potential tensile residual stresses in the stir zone and the brittle cleavage texture, the stresses that were released from clamping of the 1 mm thick 14YWT plate may have initiated cracks near submicroscopic defects produced by the spinning pin tool during FSW. The large crack that emanated from the bottom surface of the thin plate shown in Figure 8 most likely was due to distortions caused by differences in thermal relaxation from high-temperatures in the stir zone and the clamping forces of the plate. It is interesting that a crack formed near the internal tip of the large crack and propagated horizontally toward the BM away from the SZ. This observation is consistent with the delamination fracture mechanism.

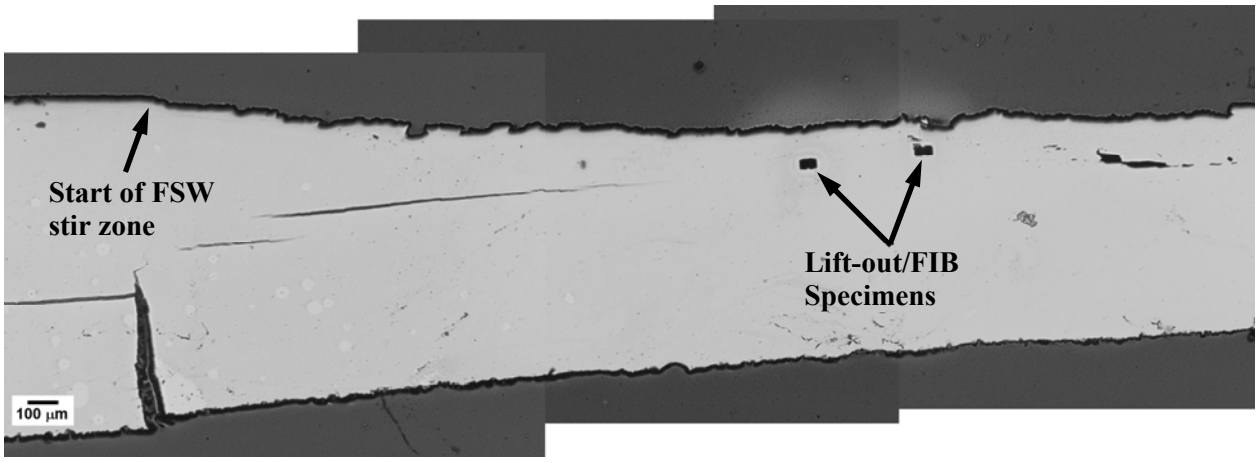

Figure 8. Composite of three OM images at higher magnification showing the cracks and pores and the location of the 2 lift-out/FIB specimens on the retreating side of the weld.

While attempting to fabricate a SS-1 tensile specimen by electro-discharge machining (EDM) that spanned across the SZ from one BM side to the other BM side of the 1 mm thick 14YWT plate, a pop-in crack suddenly occurred that fractured the plate into two sections as shown in Figure 9. The cause of the crack initiation and rapid propagation was most likely due to residual stresses as supported by recent studies of

residual stresses in FSW welds [1-4]. However, it is not clear if the residual stresses that led to the brittle crack in the 1 mm thick 14YWT plate were generated entirely in the SZ during FSW or may have also accumulated during severe deformation caused by the series of hot rolling runs to produce the 1 mm thick 14YWT plate.

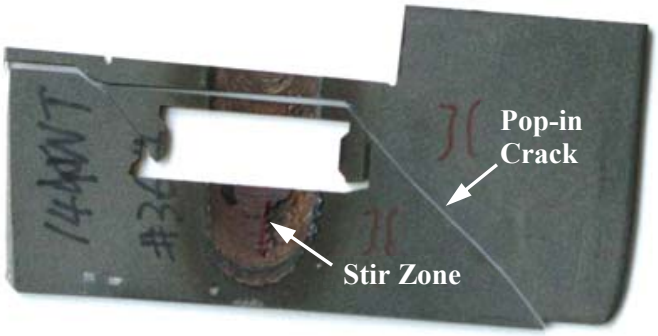

Figure 9. The 1 mm thick 14YWT plate following the abrupt pop-in crack that occurred during fabrication of the SS-1 tensile specimen by wire EDM.

The neutron scattering experiments were conducted on four plates of 14YWT-SM13 that were rolled from the starting thickness of 10 mm (R1 plate) to the final thickness of 1.0 mm (R4 plate) for the friction stir weld study. Figure 10 shows images of the R2, R3 and R4 plates after being rolled to thicknesses of 5 mm (Fig. 10a), 2.2 mm (Fig. 10b) and 1.0 mm (Fig. 10c), respectively, for deformation magnitudes corresponding to 76%, 89% and 95%, respectively. The neutron scattering experiments first involved determining the maximum scattering intensity from a bell-shaped histogram obtained with a linear scan through the thickness direction of each plate. The scanning experiments were then performed using a 2-dimensional grid of points (s_x and s_y) on the surface of the plates at a depth in the plate corresponding to the maximum scattering intensity (s_z). The {112} bcc-Fe peak was selected for the scanning runs, which were performed with the plates oriented in the extrusion direction (ED), rolling direction (RD) and normal direction (ND). Since the neutron scattering intensity for each data point depended on the thick of the plate, the scan times were considerable longer for the experiments on R3 and R4 compared to R1 and R2 to obtain good signal-to-noise ratio in the data. This was achieved by varying the total number of data points collected in the 2-D grids. Thus, the grid sizes used in the scattering experiments were 9 x 7 (R1), 11 x 8 (R2), 5 x 3 (R3) and 5 x 3 (R4), which corresponded to 63, 88, 15 and 15 number of data points, respectively.

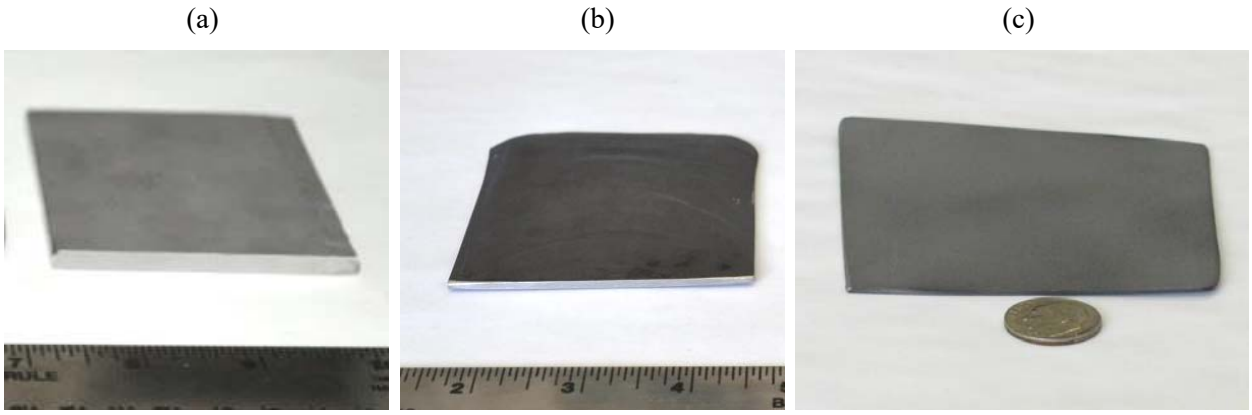

Figure 10. Digital images of the (a) 5 mm thick R2 plate, (b) 2.2. mm thick R3 plate and (c) 1.0 mm thick R4 plate of 14YWT-SM13.

The full-width half-maximum (FWHM) of the {112} neutron scattered peak for the 4 rolled plates are shown in Figure 11. The position shown on the x-axis corresponds to the 2-D grid of data points, so that groups of data correspond to rows and columns in the grid and the total number of data points depend on the size of the grids mentioned previously. Some of the data points were eliminated due to low scattering intensity and poor signal-to-noise ratio. In Figure 11a, the FWHM of the ED orientation is shown for the four rolled plates. The FWHM values fluctuate with position on the 2-D grid of data points. The results showed that the FWHM are similar for R1 and R2 and are continuously decreasing for R3 and R4, with the latter having the lowest value. Peak broadening, as measured by FWHM, is caused by a reduction in crystallite size, i.e. grain size, and/or an increase in microstrains, i.e. dislocation density, during plastic deformation. However, plastic deformation during rolling will expand the grains of the microstructure in the extrusion and rolling directions, but will compress the grains in the thickness direction, resulting in changes to the grain aspect ratio (GAR). The effective increase in grain size in the extrusion and rolling directions results in the lower FWHM for the ED orientation, which is opposite of peak broadening. The FWHM of the ND orientation for the four plates is shown in Figure 11b. In this case, the thickness of the grains will decrease as the rolling deformation magnitude increase, which is consistent with the results by showing a small, but steady, increases in FWHM values from R1 to R4. Thus, the FWHM data indicate how the grain morphology evolves during plastic deformation by rolling. Nevertheless, some variations in FWHM may also be due to microstrains introduced by dislocations during plastic deformation.

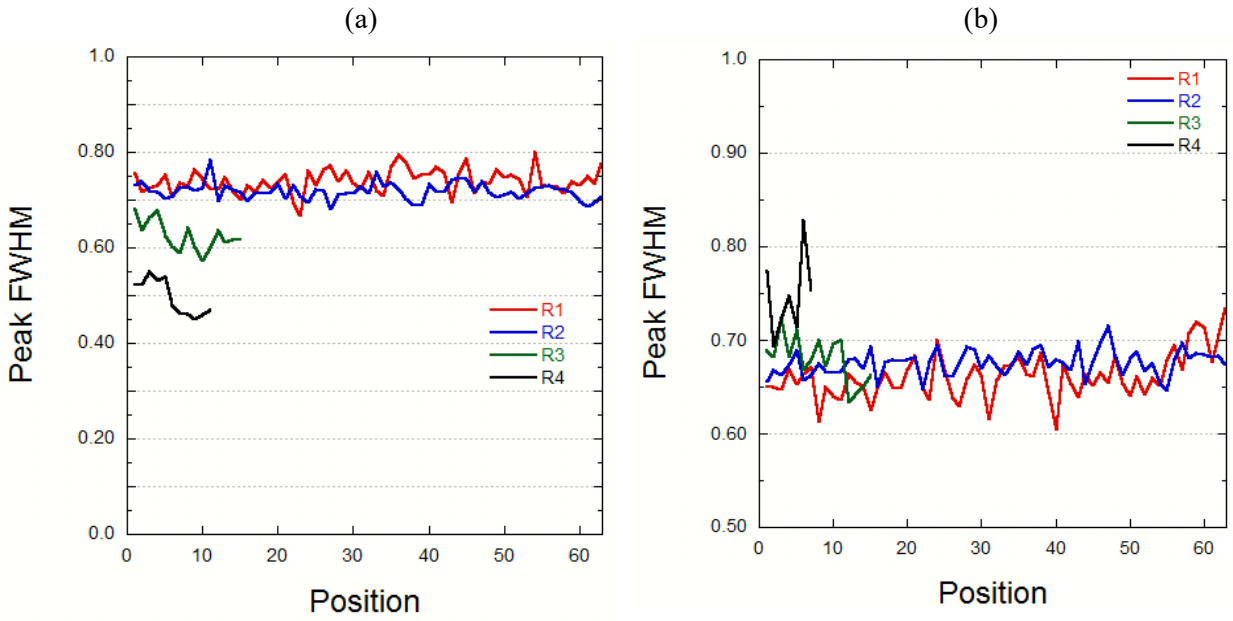

Figure 11. Distribution of FWHM of {112} peaks with position comparing R1, R2, R3 and R4 plates in the (a) ED orientation and (b) ND orientation.

The residual strains measured for the {112} peaks were obtained from the neutron scattering experiments. The d-spacing of the {112} planes were determined from the data and used in calculating the lattice strain using the following equation:

$$\varepsilon = \frac{d_{hkl} - d_0}{d_0}$$

where, d_{hkl} is the measured d-spacing of {112} from the scattering experiments and d_0 is the reference d-spacing of {112} usually obtained from an unstrained sample. Thus, the lattice strain is due to the change

in {hkl} peak position from the stress-free location in sample. In this experiment, a stress-free sample was not used. Since the stress-state is constant in each rolled plate, a stress-free region could not be used either. For this report, the reference d_0 was calculated from the average d-spacing of {112} planes in the R1 plate since this plate had the lowest deformation magnitude. Therefore, the calculated values of residual strains and ultimately residual stresses will underestimate the actual values. However, a more accurate d_0 will be determined in a future neutron scattering experiment using an annealed sample of 14YWT-SM13 in the as-extruded condition.

The distribution of residual strains with data point obtained for the four rolled plates are shown in Figure 12. Each plot shows the residual strains that were measured in the ND, ED and RD orientations with the

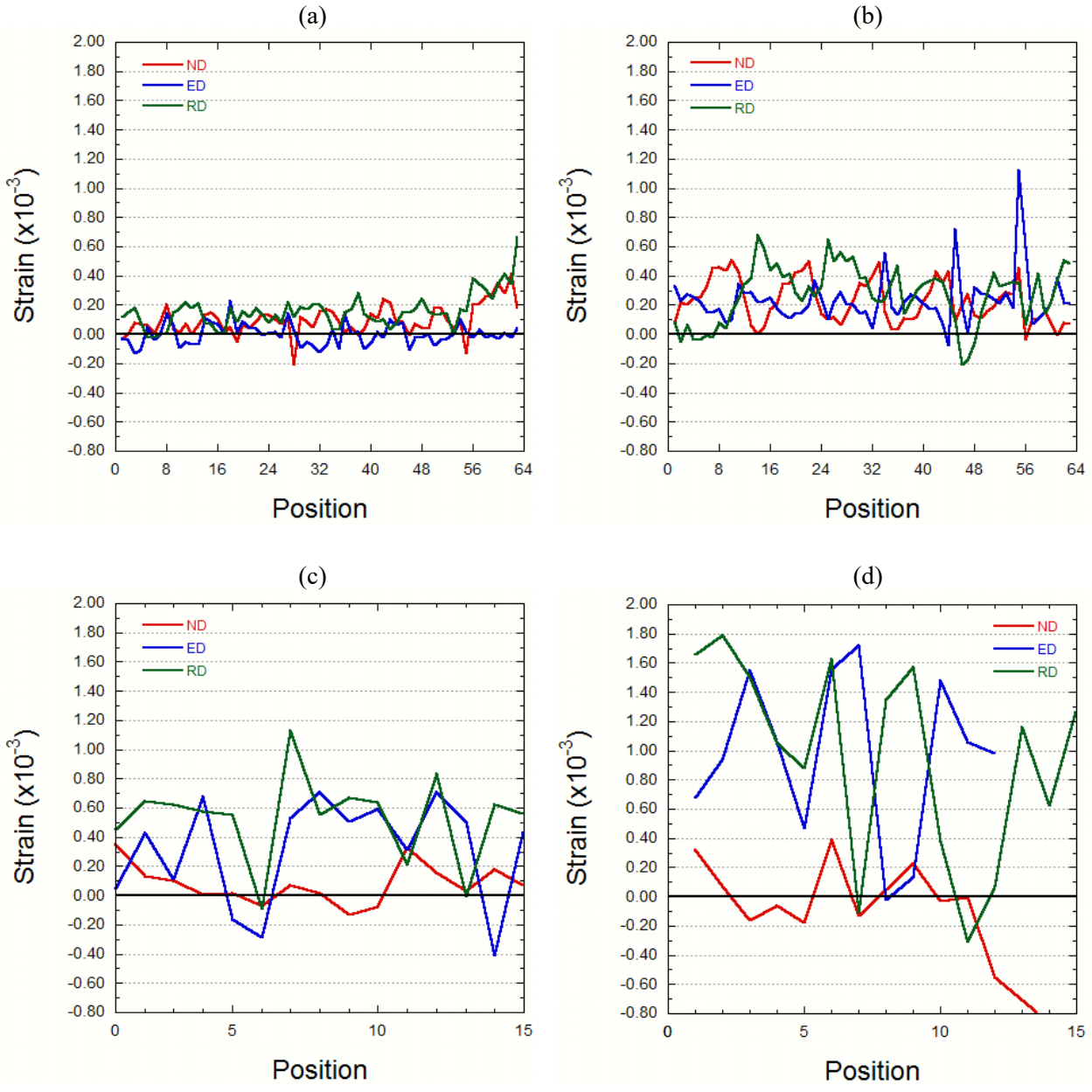

Figure 12. The distribution of residual strains with the data points for the ND, ED and RD orientations for the (a) R1, (b) R2, (c) R3 and (d) R4 plates of 14YWT-SM13.

coordinates ranging from -0.8 to 2.0 on the y-axis. The residual strains fluctuate mostly about zero strain, shown as the black horizontal line, indicating tensile rather than compressive components of strain. The fluctuations increase in amplitude with increasing deformation and are the largest in the R4 plate. Figure 13 compares the residual strains of the four rolled plates grouped into the scanning orientations of ED, RD and ND. What becomes clear in these plots is that the residual strains continually increase with increasing deformation magnitude for the extrusion (Fig. 13a) and rolling (Fig. 13b) directions, but remain effectively unchanged for the normal direction (Fig. 13c). These results are consistent with plastic deformation occurring in plane during rolling. This indicates that the residual strains occur mainly in plane and are confined to the extrusion and rolling directions.

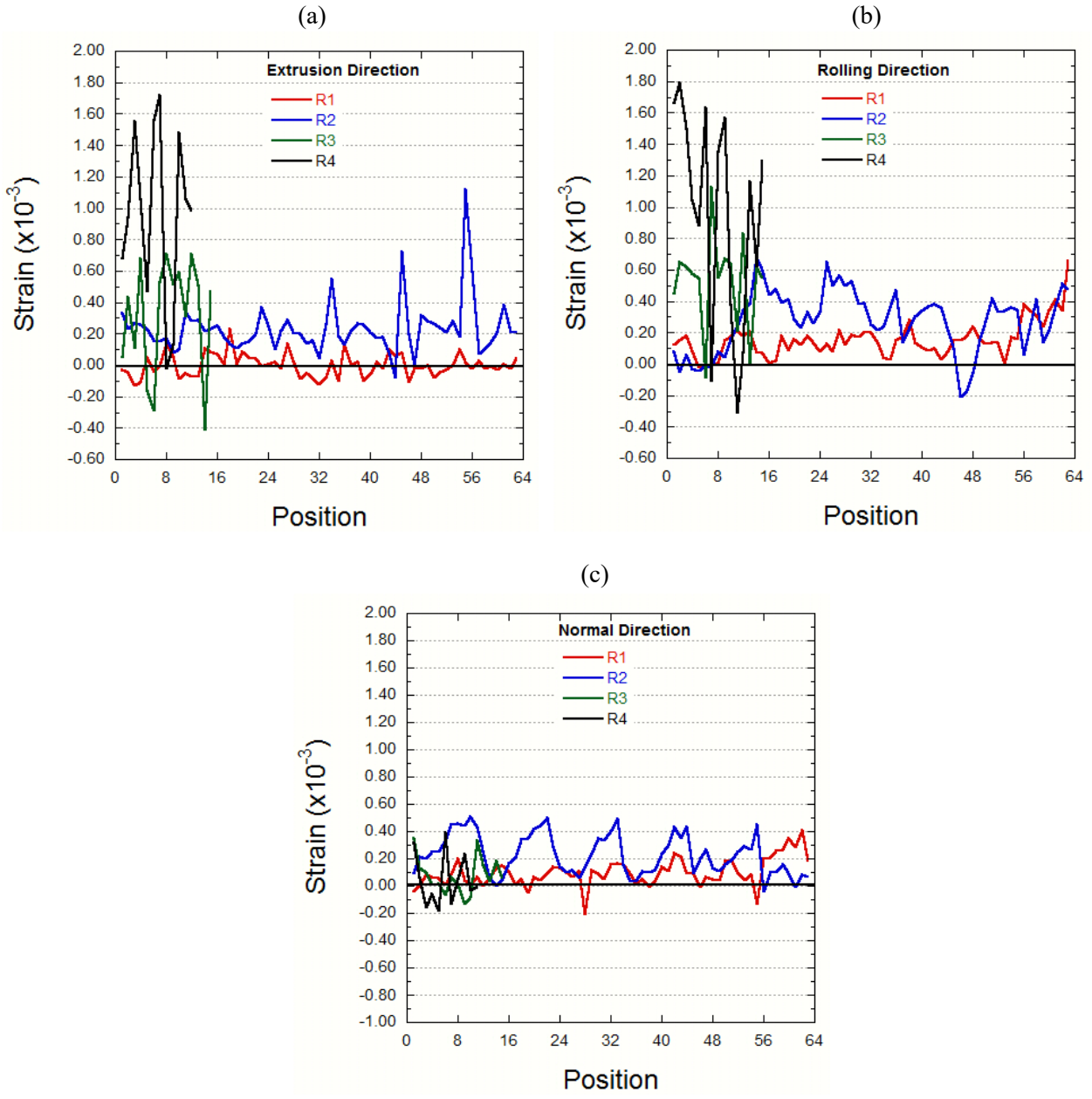

Figure 13. The distribution of residual strains with the data points for the R1, R2, R3 and R4 plates of 14YWT-SM13 measured in the (a) ED, (b) RD and (c) ND orientations.

An estimate of the residual stresses in the R4 plate was determined from the residual strains using the simple Hooke's law:

$$\sigma_{ij} = \frac{E^{hkl}}{(1+\nu^{hkl})}\left\{\varepsilon_{ij} + \frac{\nu^{hkl}}{1-2\nu^{hkl}}\left(\varepsilon_{11}^{hkl} + \varepsilon_{22}^{hkl} + \varepsilon_{33}^{hkl}\right)\right\}$$

where E^{hkl} is the Young's Modulus, ν^{hkl} is the Poisson's Ratio and ε_{ij} is the measured lattice strain in a given direction in the plate. Values of E^{hkl} and ν^{hkl} were recently obtained for 14YWT-SM13 by in-situ uniaxial tensile tests with high-energy synchrotron X-ray diffraction experiments at the 1-ID beamline at the Advanced Photon Source at Argonne National Laboratory [7]. At room temperature, the value for E^{hkl} was ~207 GPa and for ν^{hkl} was ~0.20. The principal strains are ε_{ii}, but in this work the lattice strains are taken as the extrusion direction for ε_{11}, the normal direction for ε_{22} and the rolling direction for ε_{33}. The residual stress values calculated for the ED orientation that were obtained from the lattice strains for R4 were found to fall within the range of ~122 - 384 MPa. This result indicates that substantial residual stresses were present in the 1 mm thick plate of 14YWT-SM13 that was used in the initial FSW bead-on-plate weld. It is likely that the values of residual stress will increase some level when a reference d_0 for the {112} peak is obtained from an unstrained sample of 14YWT in the future that will help refine the residual strain data.

SUMMARY

The investigation of the bead-on-plate stir zone (SZ) weld produced on the 1 mm thick plate of 14YWT by friction stir welding continued. The tensile properties and plastic deformation behavior of the SZ and base metal (BM) were investigated using digital image correlation (DIC) during in-situ tensile testing of miniature tensile specimens to assess the quality of the FSW parameters used in the initial experiment. The results of the DIC analysis of the tensile tested miniature specimens showed that the strength properties of specimens from the SZ decreased ~13% compared to specimens from the BM, but that the ductility properties were essentially unchanged by FSW. All specimens exhibited similar deformation behavior that consisted of increased intensity of strain localization and local strain rates in the region of the specimen gauge where necking occurred until the specimen failed. The results suggested that deformation bands may be slightly more prevalent during deformation in specimens from the stir zone compared to the unaffected zone.

The microstructural analysis of the SZ reported in the FY16 milestone report indicated that several cracks oriented horizontally to the plane of the thin plate were observed in the SZ, thermal mechanically affected zone (TMAZ) and BM on the retreating side of the weld. These cracks may have formed by the combination of stress introduced by friction stir welding (FSW) from clamping and residual stresses from FSW in the weld. For this reason, a HFIR Neutron Scattering User proposal was submitted and accepted for investigating residual stresses in the four plates of 14YWT (SM13 heat) that were produced during fabrication of the 1 mm thick plate. The results showed that residual strains accumulated in each plate with increasing rolling deformation magnitude. The dependence of the residual strains on orientation within the plates was obtained by scanning each plate in the extrusion (ED), rolling (RD) and normal (ND) directions. The results indicated that residuals strains increased in ED and RD with increasing deformation magnitude but were insensitive to the deformation magnitude in ND. This observation was consistent with deformation occurring in plane in the plates during rolling. The estimate of residual stresses in the final 1 mm thick plate of 14YWT used in the FSW study showed a range in values from ~122 - 384 MPa, which is a substantial amount of stress that could account for the pop-in crack that occurred during fabrication of tensile specimens for the DIC study. Additional residual stress measurements are planned in the next FY work package that will investigate the SZ to determine what how much residual stresses are produced by FSW and will study what effects post weld heat treatments have on reducing the residual stresses.

REFERENCES

[1] M.N. Gussev, R.H. Howard, K.A. Terrani and K.G. Field, Nuclear Engineering and Design, 320, (2107) 298-308.

[2] M.H. Mathon, V. Klosek, Y. de Carlan and L. Forest, Journal of Nuclear Materials, 386-388 (2009) 475-478.

[3] L.N. Brewer, M.S. Bennett, B.W. Baker, E.A. Payzant and L.M. Sochalski-Kolbus, Materials Science & Engineering A, 647 (2015) 313-321.

[4] P.J. Withers and H.K.D.H. Bhadeshia, Materials Science and Technology, 17(4) (2001) 366-375.

[5] P. Ji, Z. Yang, J. Zhang, L. Zheng, V. Ji and V. Klosek, Journal of Materials Science, 50 (2015) 7267-7270.

[6] M.E. Alam, S. Pal, K. Fields, S.A. Maloy, D.T. Hoelzer and G.R. Odette, Materials Science & Engineering A, 675 (2016) 437-448.

[7] Y. Gan, K. Mo, D. Yun, D.T. Hoelzer, Y. Miao, Z. Liu, K-C. Lan, J-S. Park, J. Almer, T. Chen and H. Zhao, Materials Science & Engineering A, 692 (2017) 53-61.